A new spin on protein dynamics

Linda Columbus and Wayne L. Hubbell

Site-directed spin labeling is a general method for investigating structure and conformational switching in soluble and membrane proteins. It will also be an important tool for exploring protein backbone dynamics. A semi-empirical analysis of nitroxide sidechain dynamics in spin-labeled proteins reveals contributions from fluctuations in backbone dihedral angles and rigid-body (collective) motions of α helices. Quantitative analysis of sidechain dynamics is sometimes possible, and contributions from backbone modes can be expressed in terms of relative order parameters and rates. Dynamic sequences identified by site-directed spin labeling correlate with functional domains, and so nitroxide scanning could provide an efficient strategy for identifying such domains in high-molecular weight proteins, supramolecular complexes and membrane proteins.

Wayne L. Hubbell*
Jules Stein Eye Institute and Dept Chemistry and Biochemistry,

Linda Columbus
Jules Stein Eye Institute, University of California, Los Angeles, CA 90095, USA.
*e-mail: hubbellw@jsei.ucla.edu

It has long been known that proteins are dynamic structures, but a connection between dynamics, stability and biological function has been recognized only recently. As a result, there is currently an intense effort to elucidate the dynamic modes of proteins in their native environment. Although the static structures derived from protein crystallography cannot provide a direct view of protein motions, they can offer clues to dynamic modes in solution. For example, different molecules in an asymmetric unit, or molecules in different crystal forms, sometimes have different conformations, raising the possibility that the protein could switch between the conformations in solution. Indeed, conformational switching is one dynamic mode underlying function that has been observed for small proteins in solution by nuclear magnetic resonance (NMR). Recent examples include structural changes related to activation in a bacterial signaling protein [1], and the movement of flaps or entire domains that control the access of substrates and products to the active sites of enzymes [2–4]. Conformational switching has also been observed in membrane proteins using site-directed spin labeling (SDSL) [5,6]. Examples include a helix-tilting motion that leads to rhodopsin activation [7], a pH-gated structural change in the KcsA bacterial K^+ channel [8] and a local unfolding in the bacterial transporter BtuB upon binding of the vitamin B12 substrate [9]. The timescale of conformational switching is generally in the micro- to millisecond range.

A second dynamic mode of a protein involves local backbone fluctuations (LBFs) in the protein at equilibrium, either as rigid-body motions of secondary structure elements or as oscillations about backbone dihedral angles. The existence of highly flexible sequences in a protein can sometimes be inferred from spatial disorder in a crystal structure, although ordering with respect to crystal contacts can be problematic. It is significant that disordered sequences observed in crystal structures have been correlated with protein–protein or protein–nucleic-acid interaction sites [10–12], and so the structure and dynamics of such sequences in solution is of functional interest.

In solution, NMR measurements of ^{15}N relaxation times have provided quantitative information on LBFs. The relaxation of protonated ^{15}N nuclei in the backbone is determined by motion of the N–H bond with respect to the magnetic field. A simple model enables extraction of the amplitude and rate of bond motion from experimentally determined relaxation times [13–16]. In this model, the derived amplitude and rate of motion are expressed in terms of an order parameter, S_{N-H}, and an effective correlation time, τ_{eff}. The order parameter ranges from 0 (for spatially unrestricted motion) to 1 (for completely restricted motion). Roughly speaking, τ_{eff} is a measure of the average lifetime of a particular spatial orientation of the bond, and its reciprocal is a measure of the rate of motion. For helical structures, experimental values for S_{N-H} are typically in the range 0.8–0.9, with τ_{eff} in the pico- to nanosecond region. However, there are interesting exceptions in which sequences that are involved in protein–protein or protein–small-molecule interactions have significantly lower order parameters, indicating dynamic disorder owing to LBFs [17–19].

Given an emerging correlation between LBF modes and function in small globular proteins, it is desirable to characterize such modes in membrane proteins and supramolecular complexes, in which the application of NMR methods is more problematic. As mentioned above, SDSL has already been used quantitatively to characterize conformational switching modes in membrane proteins and (as discussed in the following text) now offers a way to identify activated LBF modes in both soluble and membrane proteins of arbitrary molecular weight.

Detecting backbone fluctuations

How can SDSL be used to detect LBF modes? In SDSL, a nitroxide sidechain, designated R1 (Fig. 1a,b), is introduced into the protein by reacting an engineered cysteine with a selective nitroxide reagent [5]. The shape of the electron paramagnetic resonance (EPR) spectrum of R1 is determined by the motion of the nitroxide ring on the nanosecond timescale. The motion might have contributions from rotary diffusion of the protein, internal dynamic modes of the sidechain, and LBFs. Experimental conditions can usually be arranged so that contributions from protein rotary diffusion are

 0968-0004/02/$ – see front matter PII: S0968-0004(02)02095-9

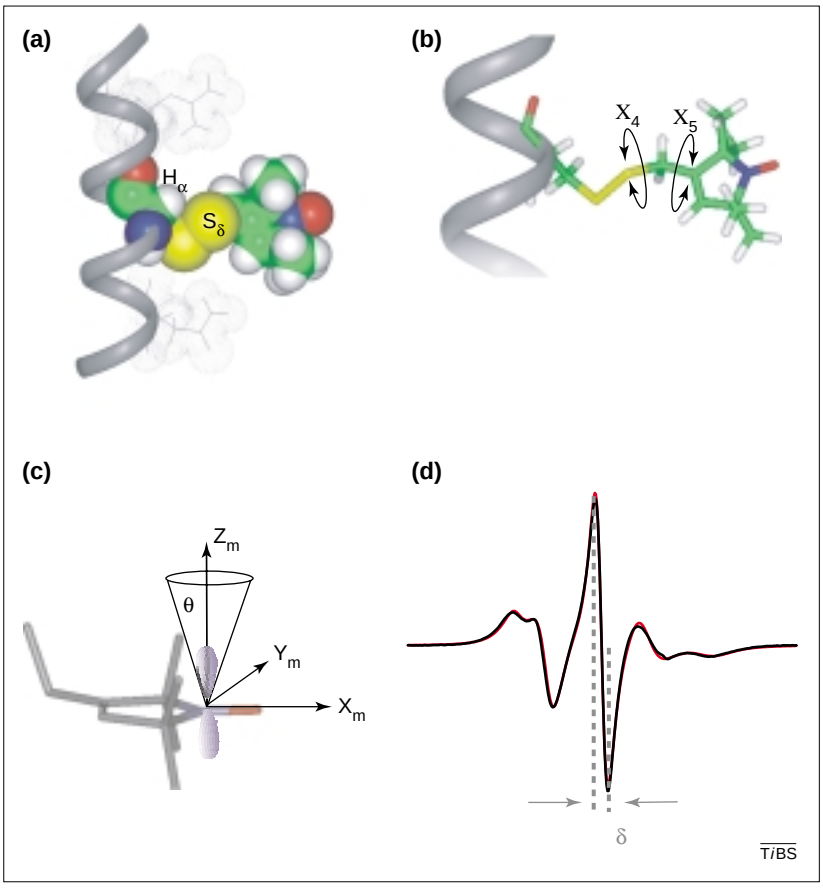

Fig. 1. Structure and dynamics of R1, a nitroxide sidechain. (a) CPK model of R1 on a solvent-exposed helix site showing the apparent interaction between S_δ and the hydrogen atom of C_α (H_α) [21]. (b) A stick model of R1 showing the flexibility of the sidechain caused by torsional oscillations about dihedrals X_4 and X_5. (c) The molecular frame of the nitroxide (x_m, y_m, z_m), with z_m along the nitroxide p orbital, indicating the average angle (θ) made by the motion of the z_m axis (in a protein fixed frame) arising from oscillations of X_4 and X_5. For simplicity, the diffusion tensor frame is taken to be coincident with the molecular frame although, in reality, these frames are tilted with respect to one another [22]. (d) Experimental (black) and best-fit (red) spectra for 72R1 of T4 lysozyme (a solvent-exposed helix site). The theoretical fit was computed using the microscopic-order–macroscopic-disorder model [23]. This model does not require motion of the p orbital within a cone but uses a generalized restoring potential to simulate the anisotropic motion. The simple axially symmetric restoring potential used in this simulation is characterized by the order parameter $S = -1/2[(3\cos^2\theta - 1)]$. For the fit to the experimental spectrum, $S = 0.47$ and $\tau = 2$ nsec. The central line width is labeled δ and the corresponding scaled mobility (M_s) value for the experimental spectrum is 0.39. For calculation of M_s, $\delta_i = 8.4$ Gauss and $\delta_m = 2.1$ Gauss.

negligible [20]. Under these conditions, the EPR spectra reflect internal sidechain motions and LBFs only. Thus, if the R1 internal dynamic modes are known at particular sites, the contributions from LBF can be deduced.

For solvent-exposed helix surface sites, where R1 experiences no interactions with nearby sidechains, a model for the internal motion has been deduced from crystallographic data, the effects of chemical modifications of the sidechain on the EPR spectra, and fitting of the experimental spectra to models for the sidechain motion [20–22]. In this model (Fig. 1a,b), the internal motion is largely limited to torsional oscillations about dihedral angles X_4 and X_5 because of an interaction of the S_δ sulfur atom with a C_α hydrogen atom in the backbone (the 'X_4/X_5' model) [21]. Constrained torsional oscillations about X_4 and X_5 lead to anisotropic motion of the nitroxide (Fig. 1c), which can be characterized by an order parameter (S) and an effective correlation time (τ_e). Although these are equivalent to the corresponding quantities used to describe the motion of N–H bonds in NMR relaxation, they now refer to the motion of the nitrogen p orbital [L. Columbus, unpublished; 23].

Values for S and τ_e for R1 at a particular site are determined from experimental EPR spectra by fitting the spectra to the X_4/X_5 model. An example is given in Fig. 1d for 72R1 in T4 lysozyme (T4L), a 'reference site' at which the backbone is highly ordered and where the motion of R1 is assumed to have minimal contributions from LBFs [22]. An important feature illustrated by 72R1 is that internal motion of R1 at a helical site is, indeed, constrained ($S = 0.47$, whereas $S = 0$ for unconstrained motion). Therefore, the overall motion of the nitroxide remains coupled to the motion of the backbone. Because the constraints on the internal motions result from interactions within the R1 sidechain, and because R1 makes no interactions with other residues at helix surface sites, it is tentatively assumed that the internal motion of R1 is constant at all such sites. Thus, site-dependent contributions to the EPR spectra that decrease S and τ_e relative to 72R1 are assigned to LBFs.

Experimental observations are consistent with this model. For example, EPR spectra of R1 at solvent-exposed helix sites from different helices reflect a similar anisotropic motion, but with different values of S and τ_e [22]. Within the context of the model, variations of S and τ_e provide quantitative measures of LBF amplitudes and rates relative to the 72R1 reference [22] and, in principle, the analysis can be applied to any helix site. However, at the present stage of development, there are limitations to a quantitative analysis based on the fitting of experimental spectra. Reliable values of S and τ_e can only be obtained from simulation of EPR spectra at multiple frequencies; this is just starting to be done [24]. In addition, the nitroxide in R1 at helix surface sites often makes weak interactions with other groups in the protein. Although this does not alter the analysis, it does complicate fitting procedures that now must involve multiple components and possibly exchange rates between them.

For these reasons, the simple inverse of the width of the central resonance line (δ^{-1}) has been used as a semiquantitative measure of nitroxide mobility that accounts for effects of both S and τ_e [5,20,25] (Fig. 1d). For convenience, this parameter can be normalized to give a 'scaled mobility', M_s [6], which is defined as $M_s = (\delta^{-1} - \delta_i^{-1})/(\delta_m^{-1} - \delta_i^{-1})$, where δ is the width of the central resonance line of R1 at the site of interest, δ_i is the corresponding width for the most immobilized R1, and δ_m is the corresponding width for the most mobile R1 in proteins. The denominator scales the function to lie roughly between 0 and 1. The values of δ_i and δ_m are affected to some extent by the polarity of the environment and possible contributions from molecular tumbling for small proteins, but the choice

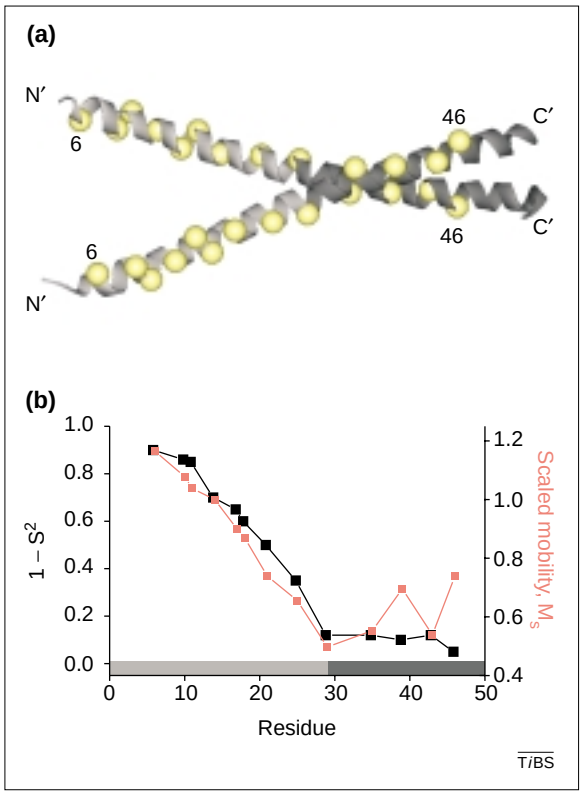

Fig. 2. Dynamics of the leucine zipper of the yeast transcription factor GCN4. (a) Ribbon diagram of the structure of the leucine zipper of GCN4 in the DNA-bound form (PDB id: 1YSA). The protein is a homodimer with the DNA-binding domain formed by the N termini (light gray ribbon). The oligomerization domain at the C terminus (dark gray ribbon) is a leucine zipper. Yellow circles at the C_α atoms indicate sites at which the R1 sidechains were introduced, one at a time. (b) The scaled mobility (M_s) from electron paramagnetic resonance (red) and $1–S^2_{N–H}$ (where $S_{N–H}$ is the order parameter for the motion of the N–H bond in the backbone) from nuclear magnetic resonance (black) of the unbound state of GCN4 are shown for the selected solvent-exposed helix sites. For calculation of M_s, $\delta_l = 8.4$ Gauss and $\delta_m = 2.1$ Gauss. Some values of M_s exceed unity because, in this case, overall tumbling of the protein contributes to apparent sidechain mobility. Molecular tumbling does not affect the internal gradient observed because the global molecular correlation time is the same for each residue.

of values does not affect the conclusions about the relative mobility of sites. M_s has the virtues of reflecting changes in both S and τ_e for the nitroxide motion, being simple to measure even in noisy spectra and not being seriously compromised by the baseline stability problems often encountered in spectra with a poor signal-to-noise ratio. In the following sections, the sequence dependence of M_s is compared with NMR data from a well-characterized system and is then used to analyze a database of published EPR spectra from soluble and membrane proteins in terms of LBFs and their implications for structure–function relationships.

Backbone fluctuations in GCN4

Does M_s reflect backbone dynamics? To answer this question, the dynamics of the backbone for the DNA-binding domain of GCN4 (Fig. 2a), as measured by NMR ^{15}N relaxation [19], were compared with M_s values obtained from R1 at the same helix surface sites (L. Columbus and W.L. Hubbell, unpublished). The NMR results are expressed as $S^2_{N–H}$, where $S_{N–H}$ is the order parameter for the motion of the N–H bond in the backbone. The quantity $1–S^2_{N–H}$, which is directly proportional to the mean-square angle of deviation of the N–H-bond vector [16], is most appropriate for comparison with M_s data. Because M_s and $1–S^2_{N–H}$ sample the same time domain, they should reveal similar features of the backbone motion. Figure 2b shows that the striking gradient in $1–S^2_{N–H}$ found in the DNA-binding domain is also revealed in M_s. Although the absolute values of the two quantities cannot be compared, a similar sequence-dependent gradient is evident in both, strongly supporting the contention that $S^2_{N–H}$ and M_s report the same physical phenomenon. The existence of a gradient in mobility increasing towards the end of the helix can be accounted for by a constant probability of a fluctuation in backbone dihedral angles along the helix, similar to the origin of the mobility gradient along the hydrocarbon chains in a lipid bilayer [26].

Apparent collective modes in α helices of soluble proteins

The channel-forming domain of the bacterial toxin colicin E1 (colE1) and the eukaryotic annexin XII are helical proteins of similar size and they bind to membranes with the appropriate stimulus but with very different mechanisms [27,28]. For colE1, irreversible insertion into bilayers to form a conductive channel is catalyzed by H^+ and involves a large-scale rearrangement of the tertiary structure [29–31]. For annexin XII, equilibrium binding to the membrane surface is mediated by Ca^{2+} and involves little or no change in the tertiary fold [32]. The function of annexin XII is not established, although it is believed to play a role in membrane fusion [28].

The M_s values for R1 throughout an 11-residue surface helix in each protein, calculated from published data [25,29], are shown in Fig. 3a. There are three outstanding features of this plot. First, the periodicity in sequence number (period ~3.6) identifies the regular helices in solution, which are as expected from the crystal structures. Second, at non-interacting helix surface sites, where the internal motions of R1 are well understood (solid symbols in Fig. 3a), M_s is similar within a given helix but differs between the two helices in the different proteins. Third, all residues within a given helix scale roughly together; that is, the tertiary contact sites and the surface sites in colE1 are much more dynamic than those in annexin.

It should be realized that the anisotropic X_4/X_5 model for R1 internal motion is not necessarily appropriate for sites in tertiary-contact interactions. Nevertheless, in view of the third point above, the use of M_s as a semiquantitative index of dynamics will be generalized to include all sites and the 'mean scaled mobility', $\overline{M_s}$, defined as the sliding average of M_s over

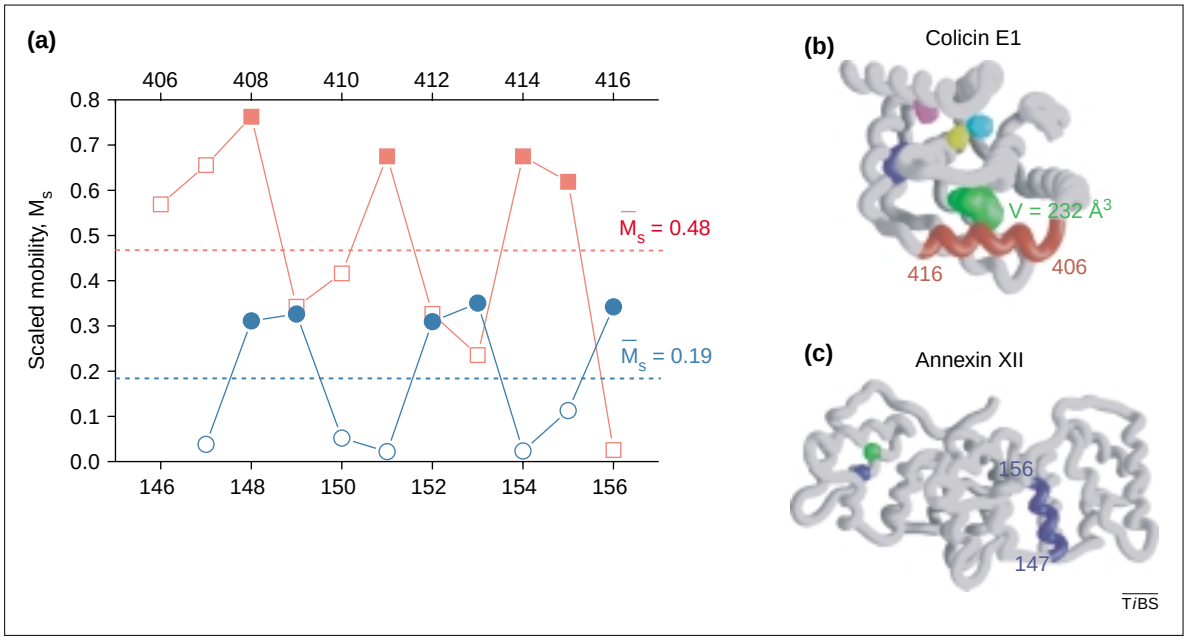

Fig. 3. Helix dynamics in colE1 and annexin. (a) The scaled mobility is plotted against the sequence for a helix in colE1 (red) [29] and annexin (blue) [25]. The mean scaled mobility for each helix, $\overline{M}_s$, is given by the dotted lines. The filled data points indicate solvent-exposed helix sites and the open data points are tertiary contact and buried sites. For calculation of M_s, $\delta_i = 8.4$ Gauss and $\delta_m = 2.1$ Gauss. (b) The structure of colE1 [30] is shown with space-filled cavities [36] in different colors; the helix analyzed in (a) (helix 401–416) is red. (c) The structure of an annexin XII monomer [58] is shown with space-filled cavities in different colors; the helix analyzed in (a) (helix 147–156) is blue.

a window of convenient length (e.g. one or two helical turns) (Fig. 3a). The fact that the M_s values for R1 at helix surface sites (and other sites) are a characteristic of the entire helix strongly suggests collective modes of motion: motion of the helix as a rigid body around one or more of three orthogonal axes [x_h, y_h and z_h (Fig. 4)].

Which collective mode could account for the differences in dynamics between the colE1 and annexin helices? Models for the R1 sidechain on helices based on crystal structures [21] and EPR line-shape analysis [22] indicate that the average orientation of the nitroxide p orbital might be roughly perpendicular to the helix axis (z_h; Fig. 4). This orientation provides maximum sensitivity to rocking motion about z_h, and this physically plausible motion might account for the differences in mobility of R1 on the colE1 and annexin helices. Assuming that this difference is caused entirely by the amplitude of rocking, the difference in angular amplitude would be ~5°, as estimated from the corresponding order parameters.

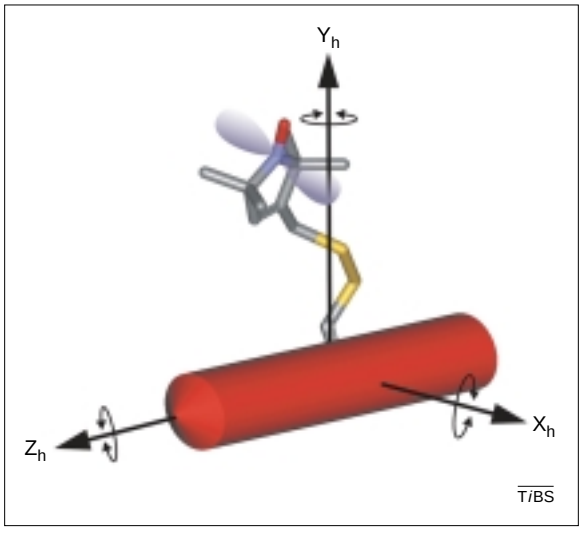

Fig. 4. Rigid-body helix motions relative to the nitroxide p orbital. A schematic view of an α helix and a model for the R1 sidechain, including a coordinate frame for defining the rigid body motions. The average orientation of the nitroxide p orbital (blue) is roughly perpendicular to the symmetry axis (z_h) of the helix.

NMR experiments designed to examine fluctuations of the N–H-bond vector (^{15}N relaxation) cannot detect rocking motions of a helix about z_h. This is because the N–H bonds lie approximately parallel to the helix axis and so the rocking motion does not result in motion of the N–H bond relative to the magnetic field, a requirement for producing relaxation. This could contribute to the near constancy of S_{N-H} in helices [33]. By contrast, C–H bonds in the backbone do not lie along z_h and ^{13}C relaxation data (which is sensitive to C–H-bond fluctuations) have been interpreted in terms of helix-rocking motions with amplitudes as large as 30° on the picosecond timescale in *Escherichia coli* flavadoxin [34]. In addition, slower (>10^{-9} s) collective motions of helices were detected in cyanometmyoglobin using residual dipolar coupling [35].

Why are helix motions more pronounced in colE1 than in annexin and is the difference related to function? Analysis of cavities in the two proteins [36] (Fig. 3b,c) reveals that helix 146–156 in annexin is well packed on its buried surface, whereas there is a large cavity (232 Å^3) in colE1, directly at the packing surface of helix 406–416. Even a small cavity reduces stability and induces measurable fluctuations in T4L [4], and it is reasonable to anticipate that helix-rocking modes with correlation times on the nanosecond timescale will be activated by packing deficiencies. It seems probable that the less-than-optimal packing (and associated dynamics) in colE1 are required for the activated molecule to sample the conformational space required for a large structural change and membrane insertion.

Apparent collective modes in transmembrane α helices

The internal dynamics of the R1 sidechain have not yet been investigated at transmembrane-helix

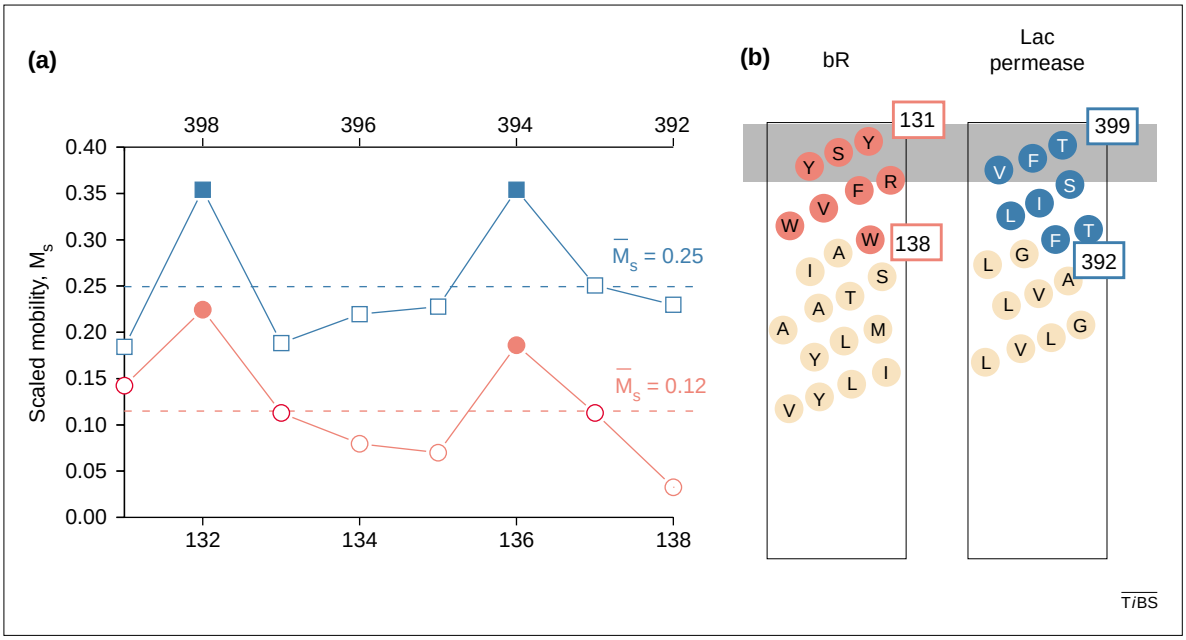

Fig. 5. Helix dynamics in bacteriorhodopsin (bR) and lac permease. (a) The scaled mobility along the 131–138 helix segment in bacteriorhodopsin (red) [40] and along helix segment 392–399 in lac permease (blue) [39]. The mean scaled mobility for each helix, $\overline{M_s}$, is given by the dotted lines. The filled data points indicate lipid-exposed helical sites and the open data points are tertiary contact and buried sites. For calculation of M_s, $\delta_i = 8.4$ Gauss and $\delta_m = 2.1$ Gauss. (b) The helical segments of bR and lac permease, showing their relationship to the membrane–aqueous interface (gray) based on site-directed-spin-labeling data.

surface sites and there is no guarantee that the motion will be similar to that observed in water-soluble proteins because of the potential importance of solvent polarity for sidechain interactions. Nevertheless, M_s reveals differences in helical dynamics similar to those observed in soluble proteins. Examples are provided by lac permease and bacteriorhodopsin. Lac permease is a bacterial H^+–β-galactoside antiporter of unknown structure, but there is abundant evidence that it is a 12-transmembrane-helix bundle [37]. Bacteriorhodopsin, a light-driven proton pump, is a seven-transmembrane-helix bundle [38]. Figure 5 shows M_s data for transmembrane-helix segments in both proteins (for lac permease, the helix structure was partly deduced by SDSL [39]). The R1 scans in each protein are the same length (eight residues) and are located at similar positions relative to the membrane–water interface [38–40]. As for colE1 and annexin, the M_s plot reveals the regular helical periodicity, and the significant differences between the values for $\overline{M_s}$ (0.25 for lac permease and 0.12 for bacteriorhodopsin) can be interpreted in terms of collective helix modes (for transmembrane helices, the motions are almost certainly collective because of the strength of the hydrogen bond in nonpolar media).

Because the structure of lac permease is unknown, it is not possible to speculate about the structural origin of the differences. However, independent studies from hydrogen exchange [41], and penetration and binding of Mn^{2+} to buried histidine residues [42], offer clear evidence for the loose packing of helices in lac permease. In addition, models of the protein indicate that helix 392–399 has only 25% of its surface interacting with a single neighboring helix [39]. By contrast, helix 131–138 in bacteriorhodopsin has contacts with two neighboring helices, leaving <50% of the helix surface exposed to lipid [38]; thus, there are few exchangeable hydrogen atoms compared with lac permease [43]. Collectively, these results are compatible with the differences in $\overline{M_s}$ between the two proteins.

As for the soluble proteins colE1 and annexin, it can be argued that the dynamic differences are related to function. The function of lac permease requires the translocation of β-galactoside across the membrane of *E. coli*, which probably requires significant internal motion in the protein. Such motions would be energetically favored in a loosely packed structure. By contrast, transport of H^+ through bacteriorhodopsin during its light-driven cycle might occur along a 'proton wire', with only small changes in structure required to prevent backflow of the proton [44].

Backbone fluctuations in rhodopsin

Rhodopsin is the prototypical G-protein-coupled receptor (GPCR) and is the only one of this large family for which a crystal structure has been obtained [11]. As for all GPCRs, rhodopsin consists of a seven-transmembrane-helix bundle, with the interconnecting segments at the cytoplasmic surface of the molecule forming the recognition domain for transducin, the visual G protein (Fig. 6a). The C terminus of rhodopsin contains phosphorylation sites that, when phosphorylated, are recognized by arrestin, inactivating the receptor [45]. The structural hallmark of light activation in rhodopsin is an outward movement of transmembrane helix 6

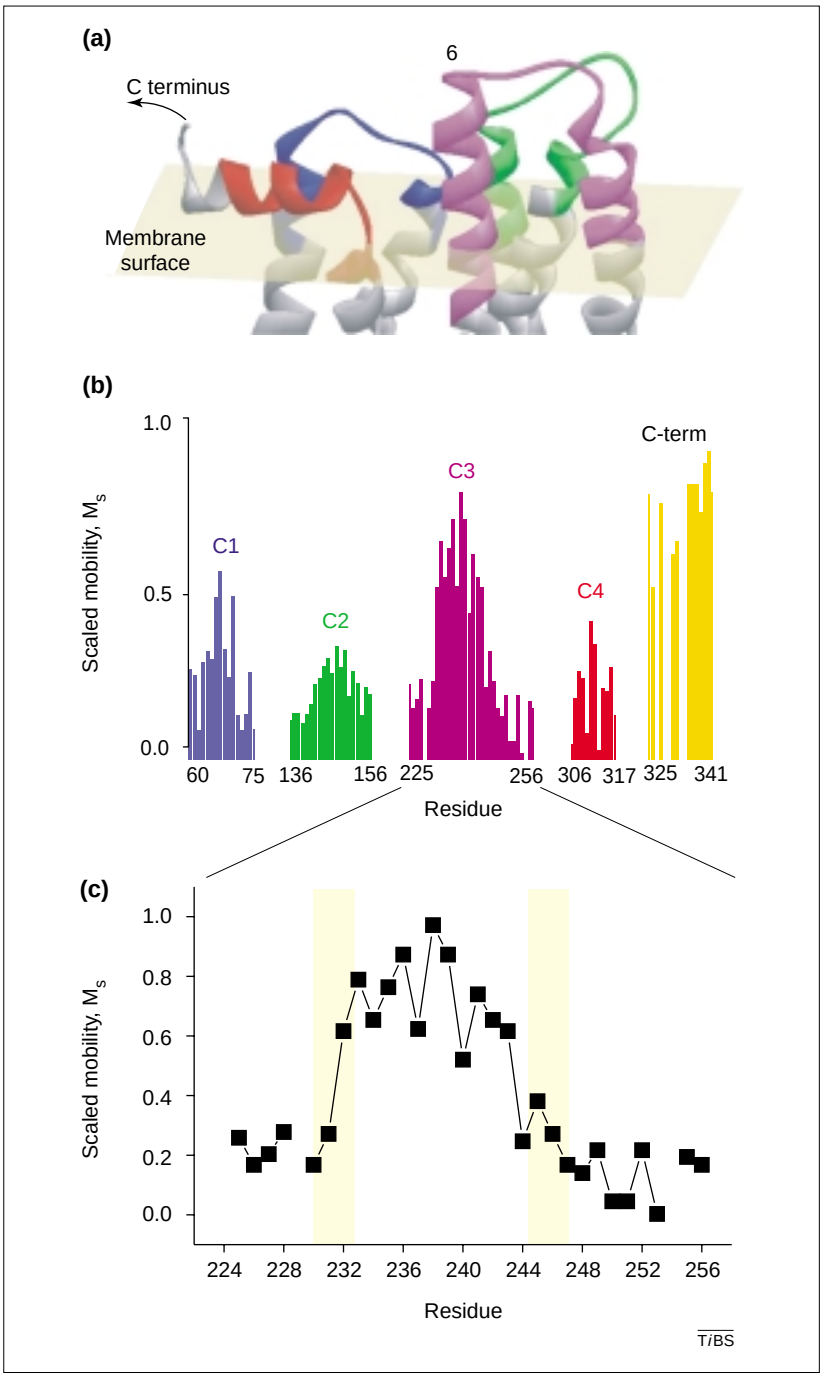

Fig. 6. Dynamics in the transducin recognition domain of rhodopsin. (a) A structural model of the cytoplasmic segments connecting the transmembrane helices (C1–C4; red, blue, magenta and green, respectively) of rhodopsin based on electron-paramagnetic-resonance data [46–50] and the X-ray crystal structure [11]. The C terminus is not shown because the structure is indeterminate along most of its length in solution [48]. (b) A plot of scaled mobility, M_s, for the entire cytoplasmic surface of rhodopsin. For calculation of M_s, $\delta_i = 8.4$ Gauss and $\delta_m = 2.1$ Gauss. The transmembrane helices are colored as in (a). (c) A more detailed plot of M_s for C3, showing the periodic oscillation that reveals its helical nature. The yellow shading indicates the lipid–aqueous interface.

(TM6) [7] (Fig. 6a) which, among other things, alters the disposition of the cytoplasmic interconnecting segments. Thus, the structure and dynamics of the cytoplasmic surface segments and the C-terminal domain (also at the cytoplasmic surface) are of primary importance for understanding the structure–function relationships in rhodopsin.

Figure 6b shows M_s values calculated from published data for the entire cytoplasmic surface of the molecule [46–50]. There are two striking features of these data: the high mobility in the central region of the third cytoplasmic segment (C3), and the high mobility throughout the C-terminal domain. The C3 segment, which is directly involved in transducin interaction, was not completely resolved in the crystal structure [11]. Moreover, the structure of this segment was clearly different in the two molecules in the asymmetric unit. Thus, this sequence has plasticity in the crystal, which is consistent with a high mobility in solution. SDSL studies showed that, in detergent micelles, C3 has a helix–turn–helix motif [46] (Fig. 6c); this is the structure shown in Fig. 6a. For residues in C3 within the bilayer (225–228 and 246–256), M_s is low, probably because of the strength of the hydrogen bond in hydrophobic media. However, from the bilayer surface to the center of the loop in the aqueous phase, there is a steep gradient of increasing M_s from either side. This gradient suggests that the dynamic mode is not a collective one but a propagated modulation of backbone dihedral angles, as for the GCN4 helix (Fig. 3). SDSL studies indicated that the C-terminal domain was unstructured, resembling a random coil [48]. Indeed, Fig. 6b shows that the C-terminal domain has the highest M_s values.

As already noted, C3 and the C-terminal domain are both key functional elements and the most mobile regions of the cytoplasmic domain. Thus, once again, dynamics measured by M_s are correlated with function. Why is high mobility of these regions important? For C3, one reason could be to permit large movements of TM6 during activation. In addition, there are transducin and rhodopsin-kinase recognition sites within C3, and the dynamics of the loop might be optimized for a high binding rate [51] and/or to limit the binding affinity caused by the large loss in entropy that would occur upon interaction of the dynamic loop with either protein. The high mobility of the C-terminal phosphorylation domain is similar to other substrates for protein kinases, in which the high mobility of the region surrounding the site of phosphorylation is probably important in recognition and affinity [52].

Conclusions

The internal motion of the R1 sidechain at helix surface sites can be characterized as a highly constrained anisotropic diffusion, and the overall motion of the nitroxide remains strongly coupled to backbone motions. Given the advanced state of EPR line-shape theory for nitroxides [53] it is, in principle, possible quantitatively to determine contributions from backbone modes to the overall motion of R1 using multifrequency EPR data, making fewer assumptions than is done in current model-free analysis of NMR data [24].

For semiquantitative applications, a scaled mobility parameter, $\overline{M_s}$, based on a nitroxide spectral

line width, identifies sequences in proteins that are dynamic on the nanosecond timescale. In addition, the sequence dependence of M_s might distinguish fluctuations in backbone dihedral angles from those caused by collective (rigid-body) modes of helices. The data suggest that the dynamic modes identified by M_s are functionally relevant. Thus, SDSL has promise as an initial screen for functional 'hot spots' by scanning selected sequences in different regions of a protein. Given a crystal structure as a starting point, SDSL also provides a simple way to map dynamic features onto an otherwise static structure. These applications are particularly attractive in view of the high time resolution (milliseconds, real-time) and the lack of any upper limit to molecular size. Moreover, the extremely small samples required (~100 picomoles of protein) makes it possible to screen proteins expressed on a small scale in tissue culture.

In addition to function, there is interest in the thermodynamic contributions of backbone and sidechain dynamics to the stability of the protein and protein complexes [54]. For these investigations, it might be useful to eliminate the internal modes of the sidechain altogether. One approach currently under investigation is the incorporation of an amino acid with the nitroxide group rigidly linked to the backbone [55]. Although this would present a significant advantage for quantitative analysis of backbone motions, it has the disadvantage that the amino acid must be incorporated synthetically or by non-native amino acid incorporation during biosynthesis [56], and no application to native proteins has been reported. Reduction of internal sidechain motion relative to R1 can also be achieved using 4-substituted derivatives of R1 that effectively lock the internal motion of the sidechain; these derivatives are just starting to be used [22]. For these sidechains, the motion should be dominated by backbone modes and it might be possible to resolve microsecond motions of the backbone using continuous wave or time-domain saturation transfer techniques [57].

Acknowledgements
We thank Christian Altenbach, John Stamm and Peter Qin for careful reading of the manuscript.

References

1 Volkman, B.F. *et al.* (2001) Two-state allosteric behavior in a single-domain signaling protein. *Science* 291, 2429–2433
2 Ishima, R. *et al.* (1999) Flap opening and dimer-interface flexibility in the free and inhibitor-bound HIV protease, and their implications for function. *Structure* 7, 1047–1055
3 Rozovsky, S. *et al.* (2001) Solution-state NMR investigations of triosephosphate isomerase active site loop motion: ligand release in relation to active site loop dynamics. *J. Mol. Biol.* 310, 271–280
4 Mulder, F.A.A. *et al.* (2001) Studying excited states of proteins by NMR spectroscopy. *Nat. Struct. Biol.* 8, 932–935
5 Hubbell, W.L. *et al.* (1996) Watching proteins move using site-directed spin labeling. *Structure* 4, 779–783
6 Hubbell, W.L. *et al.* (2000) Identifying conformational changes with site-directed spin labeling. *Nat. Struct. Biol.* 7, 735–739
7 Farrens, D.L. *et al.* (1996) Requirement of rigid-body motion of transmembrane helices for light activation of rhodopsin. *Science* 274, 768–770
8 Liu, Y. *et al.* (2001) Structure of the KcsA channel intracellular gate in the open state. *Nat. Struct. Biol.* 8, 883–887
9 Merianos, H.J. *et al.* (2000) Substrate-induced exposure of an energy-coupling motif of a membrane transporter. *Nat. Struct. Biol.* 7, 205–209
10 Sondek, J. *et al.* (1996) Crystal structure of a G-protein βγ dimer at 2.1 Å resolution. *Nature* 379, 369–374
11 Palczewski, K. *et al.* (2000) Crystal structure of rhodopsin: a G protein-coupled receptor. *Science* 289, 739–745
12 Milburn, M.V. *et al.* (1990) Molecular switch for signal transduction: structural differences between active and inactive forms of protooncogenic Ras proteins. *Science* 247, 939–945
13 Lipari, G. and Szabo, A. (1982) Model-free approach to the interpretation of nuclear magnetic resonance relaxation in macromolecules. 1. Theory and range of validity. *J. Am. Chem. Soc.* 104, 4546–4559
14 Lipari, G. and Szabo, A. (1982) Model-free approach to the interpretation of nuclear magnetic resonance relaxation in macromolecules. 2. Analysis of experimental results. *J. Am. Chem. Soc.* 104, 4559–4570
15 Palmer, A.G. *et al.* (1996) Nuclear magnetic resonance studies of biopolymer dynamics. *J. Phys. Chem.* 100, 13293–13310
16 Palmer, A.G. (2001) NMR probes of molecular dynamics: overview and comparison with other techniques. *Annu. Rev. Biophys. Biomol. Struct.* 30, 129–155
17 Crump, M.P. *et al.* (1999) Backbone dynamics of the human CC chemokine eotaxin: fast motions, slow motions, and implications for receptor binding. *Protein Sci.* 8, 2041–2054
18 Duggan, B.M. *et al.* (1999) Inherent flexibility in a potent inhibitor of blood coagulation, recombinant nematode anticoagulant protein c2. *Eur. J. Biochem.* 265, 539–548
19 Bracken, C. *et al.* (1999) Temperature dependence of intramolecular dynamics of the basic leucine zipper of GCN4: implications for the entropy of association with DNA. *J. Mol. Biol.* 285, 2133–2146
20 Mchaourab, H.S. *et al.* (1996) Motion of spin-labeled side chains in T4 lysozyme. Correlation with protein structure and dynamics. *Biochemistry* 35, 7692–7704
21 Langen, R. *et al.* (2000) Crystal structures of spin labeled T4 lysozyme mutants: implications for the interpretation of EPR spectra in terms of structure. *Biochemistry* 39, 8396–8405
22 Columbus, L. *et al.* (2001) Molecular motion of spin labeled side chains in α-helices: analysis by variation of side chain structure. *Biochemistry* 40, 3828–3846
23 Budil, D.E. *et al.* (1996) Nonlinear-least-squares analysis of slow-motion EPR spectra in one and two dimensions using a modified Levenberg–Marquardt algorithm. *J. Magn. Reson. Ser. A.* 120, 155–189
24 Barnes, J.P. *et al.* (1999) A multifrequency electron spin resonance study of T4 lysozyme dynamics. *Biophys. J.* 76, 3298–3306
25 Isas, J.M. *et al.* (2002) Structure and dynamics of a helical hairpin and loop region in annexin 12: a site-directed spin labeling study. *Biochemistry* 41, 1464–1473
26 Hubbell, W.L. *et al.* (1971) Molecular motion in spin-labeled phospholipids and membranes. *J. Am. Chem. Soc.* 93, 314–326
27 Parker, M.W. *et al.* (1990) Insights into membrane insertion based on studies of colicins. *Trends Biochem. Sci.* 15, 126–129
28 Seaton, B.A. (1996) *Annexins: Molecular Structure to Cellular Function*, R.G. Landes Co., Austin, TX, USA.
29 Salwinski, L. *et al.* (1999) Structure in the channel forming domain of colicin E1 bound to membranes: the 402–424 sequence. *Protein Sci.* 8, 562–572
30 Elkins, P. *et al.* (1997) A mechanism for toxin insertion into membranes is suggested by the crystal structure of the channel-forming domain of colicin E1. *Structure* 5, 443–458
31 Cramer, W.A. *et al.* (1990) Structure and dynamics of the colicin E1 channel. *Mol. Microbiol.* 4, 519–526
32 Langen, R. *et al.* (1998) Membrane-mediated assembly of annexins studied by site-directed spin labeling. *J. Biol. Chem.* 273, 22453–22457
33 Goodman, J.L. *et al.* (2000) Relationships between protein structure and dynamics from a database of NMR-derived backbone order parameters. *J. Mol. Biol.* 295, 963–978
34 Fischer, M.W. *et al.* (1998) Characterizing semilocal motions in proteins by NMR relaxation studies. *Proc. Natl. Acad. Sci. U. S. A.* 95, 8016–8019
35 Tolman, J.R. *et al.* (1997) NMR evidence for slow collective motions in cyanometmyoglobin. *Nat. Struct. Biol.* 4, 292–297
36 Nicholls, A.N. *et al.* (1991) Protein folding and association: insights from the interfacial and thermodynamic properties of hydrocarbons. *Proteins* 11, 281–296
37 Frillingos, S. *et al.* (1998) Cys-scanning mutagenesis: a novel approach to structure function relationships in polytopic membrane proteins. *FASEB J.* 12, 1281–1299

38 Luecke, H. *et al.* (1999) Structure of bacteriorhodopsin at 1.55 Å resolution. *J. Mol. Biol.* 291, 899–911
39 Voss, J. *et al.* (1996) Site-directed spin labeling demonstrates that transmembrane domain XII in the lactose permease of *Escherichia coli* is an α-helix. *Biochemistry* 35, 12915–12918
40 Altenbach, C. *et al.* (1990) Transmembrane protein structure: spin labeling of bacteriorhodopsin mutants. *Science* 248, 1088–1092
41 Coutre, J.L. *et al.* (1997) The lipid bilayer determines helical tilt angle and function in lactose permease of *Escherichia coli*. *Proc. Natl. Acad. Sci. U. S. A.* 94, 10167–10171
42 Jung, K. *et al.* (1995) Engineering a metal binding site within a polytopic membrane protein, the lactose permease of *Escherichia coli*. *Biochemistry* 34, 6272–6277
43 Downer, N.W. *et al.* (1986) Infrared spectroscopy study of photoreceptor membrane and purple membrane: protein secondary structure and hydrogen-deuterium exchange. *J. Biol. Chem.* 261, 3640–3647
44 Subramaniam, S. *et al.* (2000) Molecular mechanism of vectorial proton translocation by bacteriorhodopsin. *Nature* 406, 653–657
45 Kuhn, H. *et al.* (1984) Light-induced binding of 48-kDa protein to photoreceptor membranes is highly enhanced by phosphorylation of rhodopsin. *FEBS Lett.* 176, 473–478
46 Altenbach, C. *et al.* (1996) Structural features and light-dependent changes in the cytoplasmic interhelical E–F loop region of rhodopsin: a site-directed spin-labeling study. *Biochemistry* 35, 12470–12478
47 Farahbakhsh, Z.T. *et al.* (1995) Mapping light-dependent structural changes in the cytoplasmic loop connecting helices C and D in rhodopsin: a site-directed spin labeling study. *Biochemistry* 34, 8812–8819
48 Langen, R. *et al.* (1999) Structural features of the C-terminal domain of bovine rhodopsin: a site-directed spin-labeling study. *Biochemistry* 38, 7918–7924
49 Altenbach, C. *et al.* (1999) Structural features and light-dependent changes in the sequence 59–75 connecting helices I and II in rhodopsin: a site-directed spin-labeling study. *Biochemistry* 38, 7945–7949
50 Altenbach, C. *et al.* (1999) Structural features and light-dependent changes in the sequence 306–322 extending from helix VII to the palmitoylation sites in rhodopsin: a site-directed spin-labeling study. *Biochemistry* 38, 7931–7937
51 Spoerner, M. *et al.* (2001) Dynamic properties of the Ras switch I region and its importance for binding to effectors. *Proc. Natl. Acad. Sci. U. S. A.* 98, 4944–4949
52 Johnson, L.N. *et al.* (1998) The structural basis for substrate recognition and control by protein kinases. *FEBS Lett.* 430, 1–11
53 Freed, J.H. (1976) Theory of slow tumbling ESR spectra for nitroxides. In *Spin Labeling Theory and Applications* (Berliner, L.J., ed.), pp. 53–132, Academic Press
54 Wand, A.J. (2001) Dynamic activation of protein fluctuations: a view emerging from NMR spectroscopy. *Nat. Struct. Biol.* 8, 926–931
55 McNulty, J.C. *et al.* (2000) Electron spin resonance of TOAC labeled peptides: folding transitions and high frequency spectroscopy. *Biopolymers* 55, 479–485
56 Cornish, V.W. *et al.* (1994) Site-specific incorporation of biophysical probes into proteins. *Proc. Natl. Acad. Sci. U. S. A.* 91, 2910–2914
57 Roopnarine, O. *et al.* (1998) Microsecond rotational dynamics of spin-labeled myosin regulatory light chain induced by relaxation and contraction of scallop muscle. *Biochemistry* 37, 14428–14436
58 Luecke, H. *et al.* (1995) Crystal structure of the annexin XII hexamer and implications for bilayer insertion. *Nature* 378, 512–515

Development of protein-detecting microarrays and related devices

Thomas Kodadek

There is great interest in the development of devices capable of monitoring the levels and post-translational modification states of hundreds or thousands of proteins simultaneously. One way to do this would be to create protein-detecting microarrays roughly akin to the DNA microarrays that are used for genome-wide expression studies. Two major challenges must be addressed before practical devices of this type become available. One is the development of high-throughput methods for the isolation of protein-binding compounds that will act as capture molecules in the array. The second is the optimization of methods that register binding of target proteins to the immobilized ligands in a sensitive and quantitative fashion. Progress in these areas, and some of the challenges remaining, are reviewed in this article.

Thomas Kodadek
Depts of Internal Medicine and Molecular Biology, Center for Biomedical Inventions, University of Texas Southwestern Medical Center, 5323 Harry Hines Blvd, Dallas, TX 75390-8573, USA.
e-mail: thomas.kodadek@utsouthwestern.edu

The development of DNA microarrays has enabled massively parallel studies of gene expression [1,2]. This has sparked great interest in the development of devices such as protein-detecting microarrays (PDMs) to allow similar experiments to be done at the protein level [3–5] (Fig. 1).

Why do we need PDMs? DNA microarrays have shown promise in advanced medical diagnostics. More specifically, several groups have shown that when the gene expression patterns of normal and diseased tissues are compared at the whole genome level, patterns of expression characteristic of the particular disease state can be observed [6–9]. For example, tissue samples from patients with malignant forms of prostate cancer display a recognizably different pattern of mRNA expression to tissue samples from patients with a milder form of the disease [10]. However, the technical demands of DNA microarray analysis make it poorly suited for use in standard clinical laboratories. A more attractive approach would be to monitor a few key proteins directly. These might be biomarkers identified by DNA microarray analysis. In this case, the PDM required would be relatively simple, containing only 5–10 features. A more radical approach would be to use PDMs with hundreds or thousands of features for the direct analysis of blood, sputum or urine samples. It is reasonable to suggest that the body would react in a specific way to a particular disease state and produce a distinct 'biosignature' in a complex data set, such as the levels of 500 proteins in the blood. Considerable effort will be required to validate this indirect approach to diagnostics. But, in the best case, one could imagine that in the future a single blood test could be used to diagnose most conditions.

 0968-0004/02/$ – see front matter PII: S0968-0004(02)02105-9